

Development and experimental analysis of an innovative self-cleaning low vacuum hemispherical floating solar still for low-cost desalination

Milad Mohsenzadeh, Lu Aye*, Philip Christopher

Renewable Energy and Energy Efficiency Group, Department of Infrastructure Engineering, Faculty of Engineering and Information Technology, The University of Melbourne, Vic 3010, Australia



ARTICLE INFO

Keywords:

Floating solar still
Interfacial evaporation
Capillary water supply
Self-cleaning
Remote areas
Life cycle cost

ABSTRACT

In this article, a novel floating salt rejecting solar still with a low vacuum condition on the evaporation chamber is developed and the performance is experimentally investigated. The new design adopts solar heat localization for interfacial evaporation and capillary water circulation to improve the evaporation rate and prevent the basin surface from residual salt accumulation. The basin is made in tubular structure composed of multi layers of porous foam and hydrophilic cellulose fabric for improved capillary water supply. The solar still consists of an external condensing coils coupled with the basin structure. It completely submerges into the water while the solar still is floating in the saline water reservoir (e.g. oceans). This enables the natural cooling of the condensing coils which increases the condensation rate. A low-cost hemispherical clear acrylic cover is used to capture the solar radiation from all directions on the basin. The system performance was examined under different scenarios. The system was found to generate distilled water at a daily rate of $4.3 \text{ L m}^{-2} \text{ d}^{-1}$ with the distillation efficiency of 35.6% during summer in Melbourne, Australia. The life cycle cost per litre of drinking water generated by the solar still is calculated at $4.7 \text{ US } \text{¢ L}^{-1}$ which is substantially lower than conventional solar stills. This system is expected to have a lower maintenance cost as it does not require as much periodic cleaning. The new system developed is a feasible alternative to address the water security challenge for water-stressed communities at remote areas or disaster-stricken areas with no access to an energy infrastructure.

1. Introduction

The natural resources of fresh water are increasingly scarce around the globe. The current trend of water shortage estimates that by 2025, the physical water scarcity will seriously affect the life of 1.8 billion people and cost many lives in African and Asian countries [1–3]. Currently, many communities who live at remote areas with low population densities are under economic water scarcity and cannot afford commercial desalination systems. Established technologies such as Multi-Stage Flash (MSF) and Reverse Osmosis (RO) which constitute 42% and 44% of globally installed capacity of water desalination are mainly energy-intensive and require huge centralised infrastructures [4,5]. This is financially infeasible to be deployed in such areas and highlights the importance of small scale and cost-effective solar driven desalination systems to be developed for remote areas.

Recent studies on solar thermal desalination systems using solar heat localization approach for interfacial evaporation have achieved high efficiencies [6–10]. These systems normally have a simple floating

structure made of low-cost materials and can be deployed on the surface of water without need for costly structure installations on the land [11–13]. Ni et al. [11] demonstrated a potable water generation at the rate of $2.5 \text{ L m}^{-2} \text{ d}^{-1}$ for a floating passive solar still with the entire material cost of $\$3 \text{ m}^{-2}$. The basin structure is composed of multiple layers with low-cost materials including insulation polystyrene foam and cellulose wick fabric. The top layer was made of black cellulose fabric for solar absorbing. Chen et al. [14] in a similar study, reported $1.5 \text{ L m}^{-2} \text{ d}^{-1}$ with the total cost of $\$43.5 \text{ m}^{-2}$.

In this concept, the solar heat is localized on the interface of water with air, heating only a small quantity of water instead of the whole bulk water contained in the basin (as seen in conventional solar stills) [15–22]. A floating thermal insulation layer is used to avoid conduction of heat from interface to the other parts of the water. In many studies, this layer is made of a carbon-based porous foam with a coating layer of solar heat absorber on the top [23–32]. Ghasemi et al. [24] used a double-layer structure made of polystyrene foam as a thermal insulator and exfoliated graphite as a solar heat absorber. They reported a substantial efficiency of vapour generation at 85% under the low

* Corresponding author.

E-mail address: lua@unimelb.edu.au (L. Aye).

Nomenclature		SV	salvage value [\\$]
<i>Symbols</i>		<i>Greek symbols</i>	
A	aperture area [m^2]	η	efficiency [-]
AC	Annual cost [\\$]		
AEC	annual electricity cost (AEC)		
AMC	annual maintenance cost [\\$]		
ASV	Annualised Salvage Value [\\$]		
CRF	Capital Recovery Factor [-]		
CRM	cost of reusable materials		
FAC	first annual cost [-]		
h_{fg}	latent heat of vapourisation of water [$\text{J kg}^{-1} \text{K}^{-1}$]		
i	interest rate [-]		
I	global solar radiation received on the aperture [W m^{-2}]		
LCUWC	Life-Cycle Unit Water Cost [$\$ \text{L}^{-1}$]		
\dot{m}	mass flow rate of distilled water [kg s^{-1}]		
n	project life or analysis period [a]		
SFF	Sinking-Fund Factor [-]		
<i>Subscripts</i>		<i>Abbreviations</i>	
s	still	EPS	expanded polystyrene
w	distilled water	ETCs	evacuated tube collectors
		EVA	ethylene-vinyl acetate
		FHSS	Floating Hemispherical Solar Still
		NVD	Natural Vacuum Desalination
		PSS	Passive Solar Still
		RPSS	Reference Passive Solar Still

concentrations of solar radiation ($<10 \text{ kW m}^{-2}$). In other study, Liu et al. [25] used expanded polystyrene (EPS) foam wrapped by carbon-coated paper. They achieved a high rate of solar-induced evaporation at $1.28 \text{ kg m}^{-2} \text{ h}^{-1}$ with the thermal conversion efficiency of 88% under one sun illumination. In a recent study, Wu et al. [27] recorded $2.63 \text{ kg m}^{-2} \text{ h}^{-1}$ evaporation rate with over 96% energy efficiency for a 3D printed biomimetic structure made of a composite resin. A passive solar still (PSS) incorporating this structure on its basin generated potable water at $1.72 \text{ kg m}^{-2} \text{ h}^{-1}$ under one sun radiation.

In addition to the solar heat localization, the structure needs to be equipped with a salt rejecting mechanism to prevent the accumulation of salt on the interface and keep the basin surface clean. Ni et al. [11] used a hydrophilic cellulose fabric to continuously lift up water to the top surface and reject extra concentration of salt back into the bulk water. This is the same mechanism as seen in plant roots, which has inspired several studies in their design of floating solar still [14,33–39]. Li et al. [33] used a porosity-tunable structure composed of a porous crosslinked polyvinyl alcohol layer for capillary water supply and nanocarbon coating for absorbing the solar radiation. By controlling the capillary height and porosity, they reached an evaporation rate of $1.67 \text{ kg m}^{-2} \text{ h}^{-1}$ under one sun illumination. Chen et al. [14] used cellulose fabric to create vertical channels distributed around a thermal insulation sheet to lift water. The experiments on this bionic floating solar still has showed the maximum evaporating temperature of 59°C and the water generation rate of $1.5 \text{ kg m}^{-2} \text{ h}^{-1}$ during the day. Zhao et al. [30] used a hybrid hydrogel made of polyvinyl alcohol as a hydrophilic layer with internal capillary channels and reduced graphene oxide as a solar absorber. The test results demonstrated a high rate of evaporation at $2.5 \text{ kg m}^{-2} \text{ h}^{-1}$ under one sun radiation.

Creating a low to high vacuum condition on the evaporation chamber of desalination systems is another approach to improve the evaporation rate of water. It enables the evaporation of water at lower temperatures, requiring less heat. Al-Kharabsheh and Goswami [40] showed that under a high vacuum pressure of 3.6 kPa , a solar still can generate potable water at 0.115 kg h^{-1} by a low-grade solar heat supply of 103 W . They used barometric pressure method to create a passive vacuum in the evaporator. In this method, the natural vacuum is created in the headspace above the column of water with the height of approximately 10.3 m . Abbaspour et al. [41] experimentally studied a natural vacuum desalination (NVD) using a high-grade solar heat supplied by evacuated tube collectors. This study recorded a water generation at the rate of $8.1 \text{ kg m}^{-2} \text{ d}^{-1}$ with the thermal efficiency of 47.6 % obtained at the vacuum pressure of 23.4 kPa (abs). The unit cost of water generation was estimated to be $\$ 0.094 \text{ L}^{-1}$. Xie et al. [42] demonstrated

a three-effect tubular solar desalination system under vacuum operation condition connected to evacuated tube collectors for the heat supply. The three-effect design is to regenerate the heat of condensation. The performance of the system was obtained for different vacuum levels, and the highest water yield reported at the operation pressure of 40 kPa was $7.1 \text{ kg m}^{-2} \text{ d}^{-1}$. The natural vacuum desalination method has been considered in several studies as an approach to reduce the power consumption of vacuum pump; however, due to the cost of vacuum pump and piping, the initial cost of high vacuum assisted desalination systems is still significant [43].

In this work, a hemispherical floating solar still with a low vacuum operation condition on the evaporation chamber is developed and the performance parameters are experimentally investigated next to a conventional passive solar still. The new design adopts localized interfacial solar heating and capillary water supply through a multi-layer basin to improve the evaporation rate and address the lingering challenge of preventing the accumulation of salt in the system. The basin consists of multi layers of hydrophilic cellulose fabric and tubular Ethylene-vinyl acetate foam. An extra condensing channels made of copper coil is coupled with the basin structure and submerged into the water while the solar still is floating in the sea or saline water reservoir. It enables the natural cooling of the condenser by the bulk water which increases the condensation rate. A low-cost hemispherical clear acrylic condensation cover is used to capture the solar radiation from all directions on the basin. A solar-powered low capacity air vacuum is used to withdraw vapour from the evaporation chamber into the condenser and creates a low vacuum condition above the basin surface. The system performance is examined and compared to a reference passive solar still. By controlling the capillary height using a simple approach, the balance between water supply and evaporation rate on the interface of the basin was maintained. This paper comprises three sections following Introduction. (1) System description and operating principles: a detailed description of the system structure and underlying concepts are presented. (2) Experiment setup: the fabricated systems, outdoor experiment procedures, measuring instruments, and indoor salt-rejection experiment are elaborated. (3) Results and discussion: the performance outcomes of the system are compared with the reference passive solar still and existing floating solar desalination systems. The conducted cost analysis results are provided, and the article is concluded by highlighting some insight on system advantages, existing shortcomings, and the future considerations.

2. System description and operating principles

2.1. Salt rejecting low vacuum hemispherical floating solar still design

Fig. 1(a) shows the structure of the basin designed to float on sea water surface to continuously wick up saltwater and localize the absorbed heat from the solar radiation received. It makes a suitable condition for interfacial evaporation of water on the surface of the basin. The floating structure is composed of several layers. A bundle of tubular expanded Ethylene-vinyl acetate (EVA) foam with a plastic tube in the middle serves as the main frame to keep the structure floating and to thermally insulate the top layer of the basin from the bulk water beneath. The foam is hydrophobic and avoids convective heat transfer, bringing the calculated thermal conductivity as low as $0.03 \text{ W m}^{-1} \text{ K}^{-1}$. A layer of super hydrophilic black fabric (**Fig. 1(b)**) wraps around the foam on the top and sinks into the water at the bottom. It acts as a wick to capillary lift the water to the interface and reject the extra concentration of salt back into the bulk water. Experiments showed this layer can absorb up to 10 times its mass in water within 2 s.

The wick layer has relatively high thermal conductivity compared to the foam; however, it comprises a relatively small part of the basin cross section as shown in **Fig. 1(a)**, therefore keeping the total effective thermal conductivity of the basin reasonably low and very close to the thermal conductivity of the foam. The top part of the black hydrophilic layer serves to absorb the solar radiation and transfer to the immediate water at the interface (**Fig. 1(c)**). The rounded geometry of the basin surface created by the tubular platform provides an extra interface area compared to the existing floating solar stills (e.g. Ref. [11–14]).

The hydrophilic fabric wick layer creates a loop of capillary water exchange between the bulk water in the reservoir and the top layer of the basin. It keeps the evaporation zone continuously wet and low in salt

concentration. This system, therefore, is expected to have a lower maintenance and operation cost compared to conventional passive solar stills due to the passive water ingress into the basin and subsequent excess salt rejection from the basin surface.

Due to the evaporation of water, the concentration of the salt at the interface increases causing a concentration difference with the bulk water in the sea. This drives reverse diffusion of high salt concentration down into the bulk water. Diffusion is the main mechanism for the rejection of excess salt through the wick layer [11]. The cross-sectional area of the wick is an important parameter to adjust the rate of capillary lifting of water and salt diffusion. This cross-sectional area is related to the solar radiation intensity and other operation parameters [11] assuming diffusion is the only mode of salt transfer. To control the level of wetness on the interface during operation in different solar radiation intensities, a simple solution is proposed with the current structure of the basin. Some water is injected into the closed-loop plastic tubes which make up the frame of the basin as shown in **Fig. 1(a)**. By changing the amount of water in the tubes (varying the weight), the floating level of the structure can be adjusted easily according to the season or climate conditions.

Fig. 2 shows the schematic views of the floating solar still. The condensation of vapour in the current structure of the floating solar still occurs in two areas: the hemispherical transparent cover on top of the basin and submerged copper coils coupled with the basin structure as shown in **Fig. 1(a)**. The hemispherical cover provides extensive area to condense part of the vapour on its inner surface via the heat loss to the ambient air whilst collecting distilled water from around the cover. The transparent cover also allows the basin to receive solar radiation from all directions and have a uniform distribution of the solar heat. The majority of the vapour in the evaporation chamber is drawn into the copper coils (**Fig. 2(c)**) to be condensed on the inner surface of the tubes and

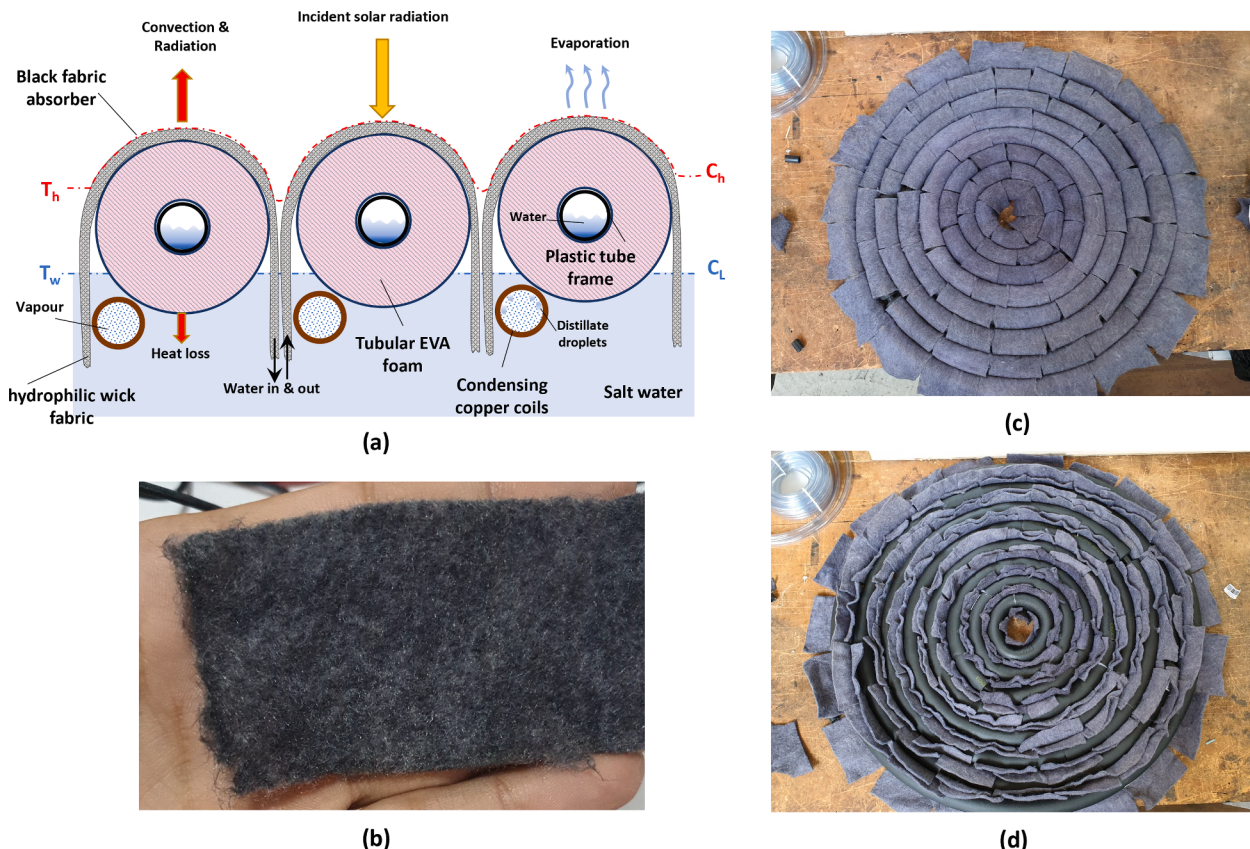


Fig. 1. (a) Schematic of the floating multi-layer basin structure, (b) The photo of the piece of super hydrophilic black wick fabric, (c) The top view of the fabricated floating basin, and (d) The bottom view of the basin.

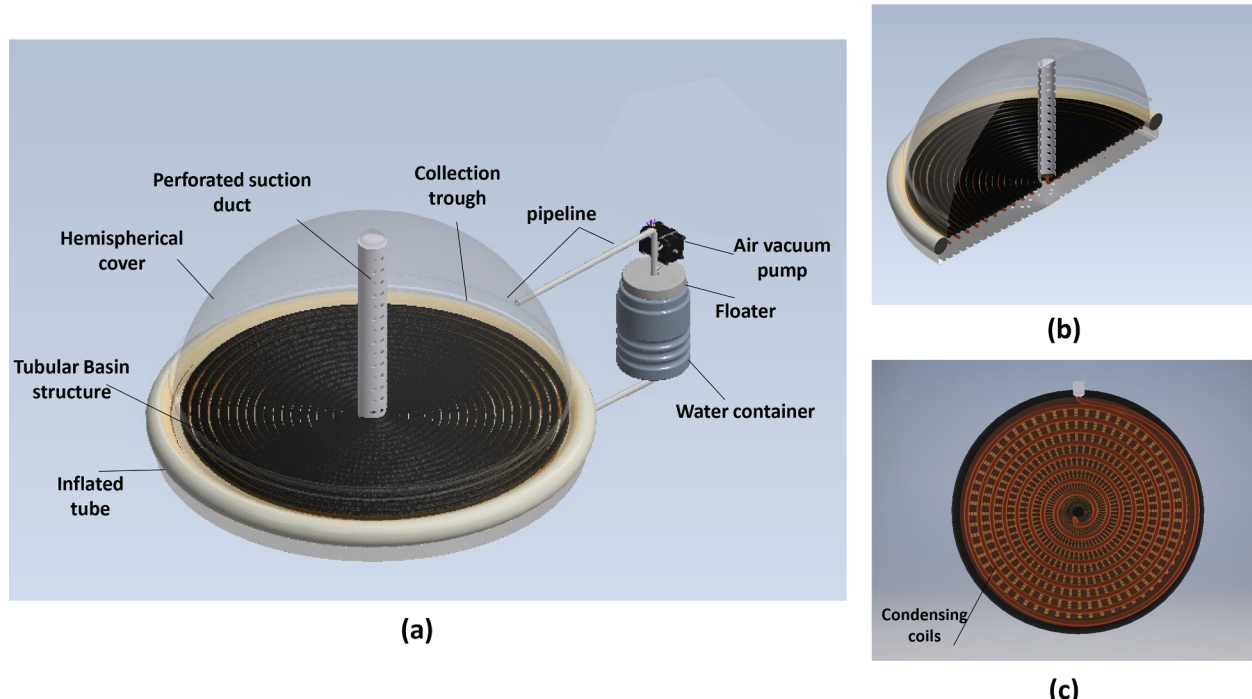


Fig. 2. The schematic of (a) the floating hemispherical Solar Still, (b) the section view of solar still, and (c) the copper coils coupled with the basin structure at the bottom of the system.

subsequently collected in a floating container. The coils are submerged into the water while the solar still is floating in the sea or saline water reservoir. This enables the natural cooling of the coils which increases the condensation rate, whilst also pre-heating the zone adjacent to the tails of the wick fabric layer.

In the condensation process, the discharged air via a PVC perforated column at the centre of the evaporation chamber ([Fig. 2\(b\)](#)) is returned after passing through the condensation coils and losing its vapour content. The air is blown over the basin surface through the openings around the hemispherical cover. This mechanism creates a low-pressure condition in the immediate vicinity above the basin surface increasing the evaporation of the heated water [[44](#)]. A low-capacity air vacuum pump is used to circulate the air between the evaporation chamber and the condensation coils as shown in [Fig. 3\(c\)](#). It takes two minutes that the device discharges the moist air from the evaporation chamber.

3. Experiment setup

[Fig. 3\(a\)](#) shows the fabricated experiment setup for the floating hemispherical solar still (FHSS). The area of the basin prepared for the outdoor experiments is 0.35 m^2 . The hemispherical cover has 700 mm diameter and 350 mm height which is made of 4 mm thick clear acrylic material. The condensing coil is made of the copper pipe with 10 mm diameter and the total length of 5 m. The details of the components used in the experiment setup are provided in [Table 1](#). The system was tested while floating in a saltwater pool with 0.5 wt% salt concentration. An inflated tube is fitted around the system at water surface level which assists in stabilising the FHSS during turbulent or windy conditions ([Fig. 2\(a\)](#)). The experiments were conducted next to a reference passive solar still in order to compare the performance parameters. The distilled water over the surface of the hemispherical cover and the condensation coils were collected in separate containers.

3.1. Reference passive solar still setup

[Fig. 3\(b\)](#) shows the fabricated reference single slope single basin passive solar still (RPSS) for outdoor tests next to the FHSS. The area of

the basin liner is 0.39 m^2 with the aspect ratio of 1:2. It is made of Galvanized Steel sheet and coloured in matte black to increase the absorption of solar radiation received. On top, a thin 4 mm clear acrylic sheet covers the evaporation chamber. It is tilted at 33° and located at 0.35 m above the basin (the average distance). The inclination of the cover was set according to the optimum value in the summer for the location of Melbourne (37.8°S , 144.9°E) in Australia [[45](#)]. The average height of the evaporation chamber (0.35 m) was chosen based on the design suggestions found in literature [[20](#)]. The structure of the chamber is made of 7 mm Plywood board. A layer of 25 mm Polystyrene foam sheet (EPS) was used as a thermal insulation on the walls and at the bottom of the system. It brings the total thickness of the walls to 40 mm with thermal conductivity of $0.021 \text{ W m}^{-1} \text{ K}^{-1}$ which is somewhat less than the average value reported ($0.056 \text{ W m}^{-1} \text{ K}^{-1}$) [[20](#)]. A V-shaped collecting trough is placed at the bottom of the cover on the front wall with a slight slope (4.5°) to collect the distilled water.

3.2. Experiment procedures

The outdoor experiments were conducted at the campus of the University of Melbourne at the location of Melbourne city (37.8°S , 144.9°E) in Australia. FHSS and RPSS are both placed in an open area facing to the North within a short distance from each other ([Fig. 3\(c\)](#)). The tests were run from 9:00 am to 17:00 pm during clear summer days in 2021. The RPSS basin was filled with 10 mm depth of water and kept at the same level by periodic refilling. The FHSS setup is placed in saltwater pool shown in [Fig. 3\(c\)](#). System temperatures were logged every second using a data logger whilst solar radiation, humidity, wind, chamber humidity, and distilled water volume was recorded every 15 min manually. The distilled water on the surface of the hemispherical cover and the condensation coils were weighed separately. The distillation efficiency of the solar still was calculated by:

$$\eta = \frac{\dot{m}_w h_{fg}}{I_s A_s} \quad (1)$$

where, h_{fg} is the latent heat of evaporation of water [$\text{J kg}^{-1} \text{ K}^{-1}$], \dot{m}_w the

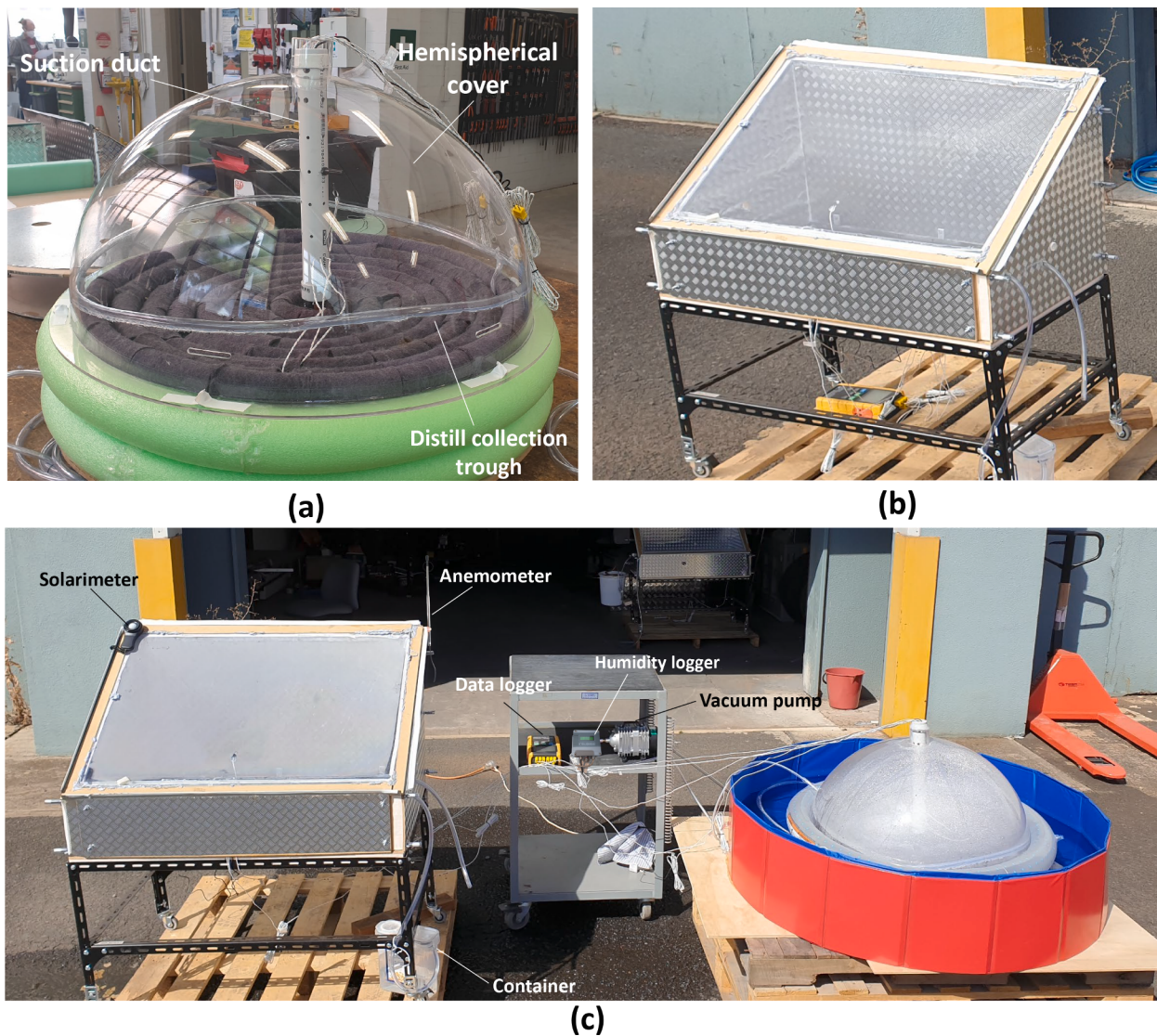


Fig. 3. Photographs of the experimental setups: (a) Floating Hemispherical Solar Still (FHSS); (b) Reference Passive Solar Still (RPSS); (c) Outdoor experiments of FHSS next to RPSS.

Table 1
The specifications of FHSS experiment setup.

Component	Material/ Brand	Dimensions
Hemispherical cover	Clear Acrylic	Semi-hemisphere, Dia. 700 mm, thickness 4 mm, 6 air inlet slots
Condensation coil	Copper tube	Outside Diameter (OD.) 3/8"(9.5 mm), coiled in 8 circles
Wick layer	Absorbent fabric	Total area of wick fabric 1.02 m ²
Insulation foam	EVA	Tubular, OD. 28 mm
Basin main frame	Poly pipe	Closed loop tubes, OD.13 mm
Suction duct	PVC	OD. 45 mm, protruded in 6 columns, 14 rows.
Distillate collecting tubes	Clear Vinyl	OD. 6 mm
Inflated ring tube	PE plastic	Ring OD. 850 mm, Tube OD. 80 mm
Air vacuum pump	Hydroponics	Rated output. 40 L/min, vacuum pressure: 35 kPa

mass flow rate of the distilled water [kg s^{-1}], I_s the global solar radiation received on the aperture area [W m^{-2}], and A_s is the aperture area of the solar still [m^2].

3.3. Measurement instruments

For FHSS experiment setup, temperatures were measured on hemispherical cover surface, evaporation chamber, basin interface (T_1), basin mid-height (T_2), water around the condensing coils (T_3), and the bulk water (T_4). The location of the thermocouples on the basin structure of FHSS are shown in Fig. 4.

4. Results and discussion

4.1. Outdoor experiments

The daily temperature distribution at different parts of FHSS and RHSS systems are shown in Fig. 4 and Fig. 5. The temperature measurements on FHSS basin (Fig. 4) showed that the average temperature of the interface during the day was 68.5°C with the maximum of 84°C. This is significantly higher than the bulk water temperature with the difference of 40°C in average. This shows the ability of the fabricated basin structure to create localised heat zone on the interface. On the other hand, RPSS has reached the maximum basin temperature of 70.5°C around 13:30 PM local time, with the average of 56.5°C which shows only 5.2°C difference with the bulk water at the basin (Fig. 5(a)).

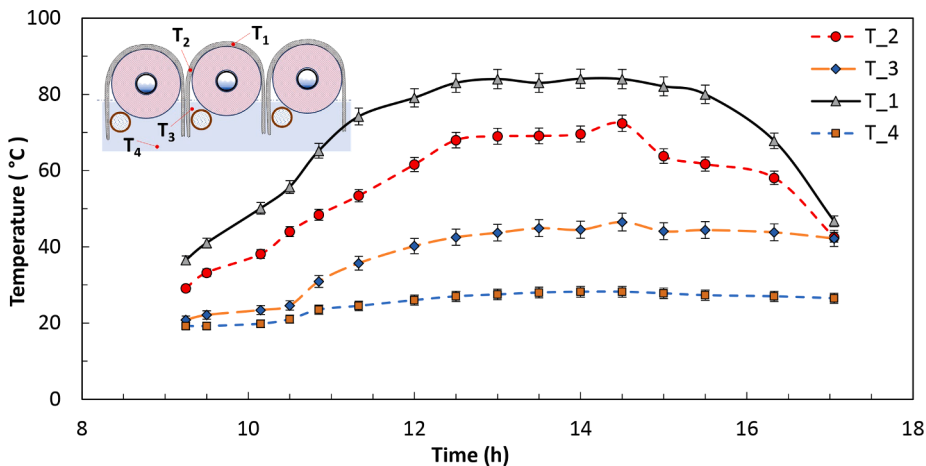


Fig. 4. The distribution of the temperature at different levels of the basin structure for FHSS system on the test date 08/Jan/2021.

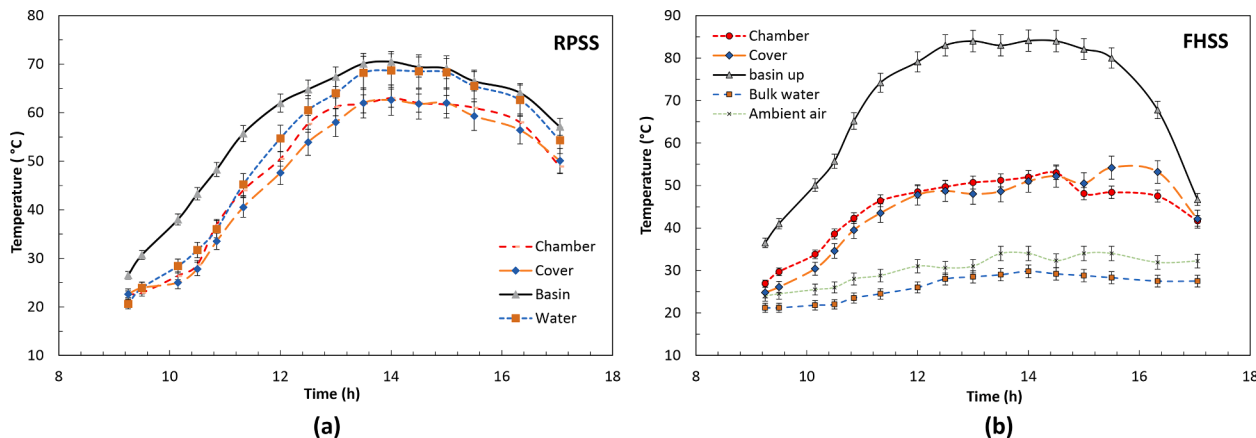


Fig. 5. The temperatures of the cover (inner side), chamber, bulk water, and the basin for (a) RPSS and (b) FHSS systems on the test date 08/Jan/2021. Clear sky with the average ambient temperature 30 °C, wind velocity 4 km h⁻¹, and relative humidity 34%.

The water temperature around the condensing coils in FHSS system was about 37°C which is 11°C higher than the bulk water inside the saltwater pool. This indicates either the positive effect of preheating the rising water on the wick layer to the interface or the negative effect of heat loss via the wick fabric back into the bulk water which needs further examinations. Table 3 provides the climate condition during the test days including ambient air temperature, wind speed, solar radiation and the humidity level.

Fig. 6(a) compares the accumulated water yield per unit area of the basin between FHSS and RPSS setups. The results show that the FHSS generates distilled water at a daily rate of 4.3 L m⁻² day⁻¹, a 64% increase in daily water yield compared to the RPSS on clear summer days with the maximum solar insulation rate of 995 W m⁻². The air vacuum pump used in the experiment took two minutes to discharge the moist air from the evaporation chamber into the condensation coils and to

return it via the air inlet slots around the hemispherical cover right above the basin surface. Fig. 6(b) shows the breakdown of accumulated water yield distilled on the cover and the coils. The hemispherical cover on top of the basin providing an extensive surface for water vapour condensation collected 23% of the total distilled water; however, the majority of the vapour condensed in the submerged copper coils coupled within the basin structure. In FHSS system, the hemispherical cover together with the condensing coils provide greater available area for condensation of the vapour compared to conventional passive solar stills. The ratio of condenser area to the basin surface for the FHSS system was 1.84, approximately 50% larger than the RPSS system ratio of 1.23.

Fig. 7(a) compares the hourly rate of water between FHSS and RPSS systems. The average rate of 0.51 L m⁻² h⁻¹ was achieved on FHSS system showing 67% increase from that of RPSS system. The FHSS took

Table 2
Type and specifications of the measurement instruments.

Measurements	Quantity	Instrument / Sensor	Instrument uncertainty	Model/Manufacturer
Incident solar radiation	1	Solarimeter	±5%	QM1582, Digitech
Temperature	12	Thermocouple (TC)	±2.2 °C	Type-K, RS PRO
Wind speed	1	Hot Wire Anemometer	±5% ± 0.3 km h ⁻¹	AM-4214SD, Lutron
Relative humidity	1	Humidity indicator	±0.1%RH	HMI31, Vaisala
Water yield	1	Digital Bench Scale	±1%	QM7264
Temperature logging	1	TC Data Logger	±0.4% ± 0.5 °C	BTM-4208SD, Lutron
TC calibration	1	Thermostatic water tank	±0.1 °C	TWBC-12, Thermoline

Table 3

The hourly climate condition, water yield, and thermal efficiency of RPSS and FHSS systems on the test date 08/Jan/2021.

Time	Climate condition				RPSS		FHSS	
	Ambient (°C)	Solar radiation (W m ⁻²)	Wind speed (km h ⁻¹)	Humidity (%)	Water yield(L h ⁻¹ m ⁻²)	Thermal efficiency (%)	Water yield(L h ⁻¹ m ⁻²)	Thermal efficiency (%)
9	23.2	545	5.2	53	0.00	0.0	0.00	0.0
10	25.5	705	7.6	46	0.12	8.3	0.04	3.8
11	28.2	879	7.2	39	0.24	14.2	0.26	18.8
12	31.0	920	4.5	33	0.47	25.0	0.21	13.8
13	31.9	996	2.4	30	0.39	20.0	0.84	53.1
14	34.8	940	4.8	25	0.34	18.3	0.91	59.5
15	34.2	880	8.2	24	0.51	29.0	0.95	67.1
16	32.9	772	4.6	25	0.24	16.6	0.52	43.4
17	32.2	564	7.4	26	0.41	33.4	0.44	44.4

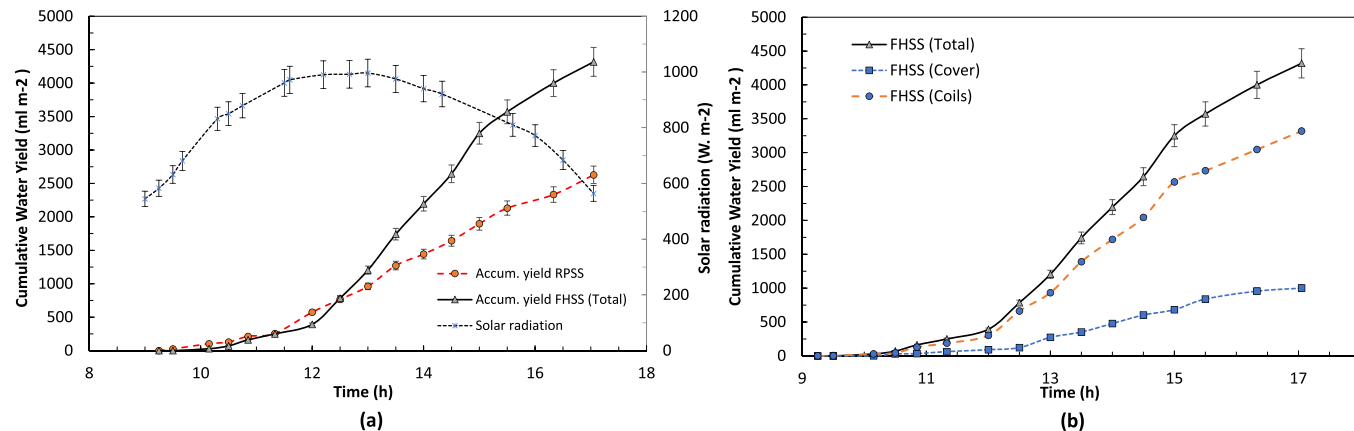


Fig. 6. (a) Comparison of the accumulated water yield per square meter of the basin between FHSS and RPSS systems, and incident solar radiation (b) Breakdowns of accumulated water yield of FHSS distilled on the cover and the coils during the test date 08/Jan/2021.

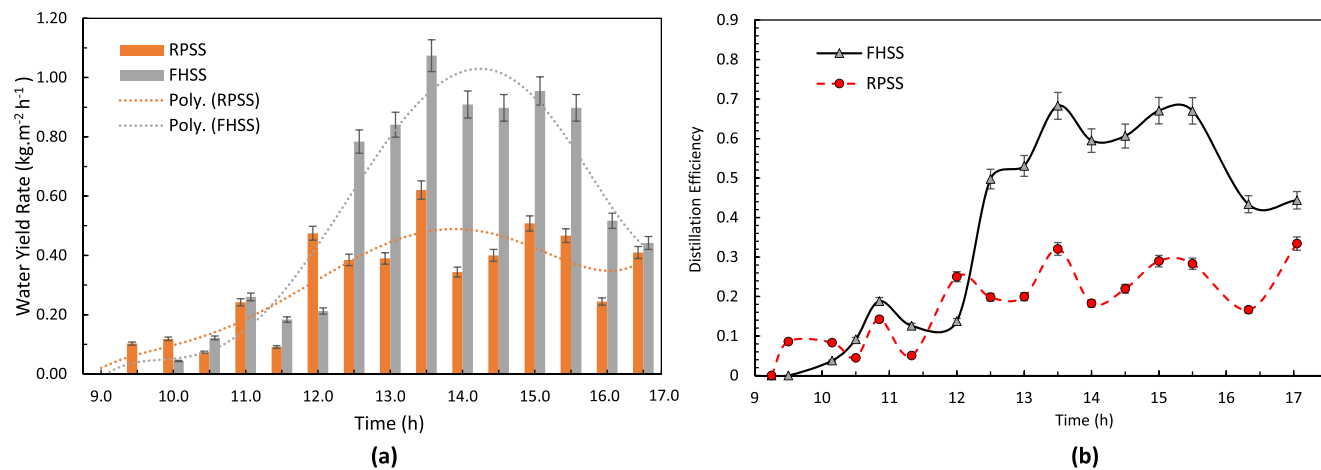


Fig. 7. Comparison of (a) the hourly rate of water yield and (b) the distillation efficiency for FHSS and RPSS on test date 08/Jan/2021.

longer to begin collecting water (~1h) compared to RPSS due to the length of the coils and collecting water pipes. However, after 12 PM, the water generation for the FHSS increases faster than that of the RPSS. This initial lag is reflected on the hourly distillation efficiency too; increased from 15% to about 50% as shown in Fig. 7(b). This indicates that probably the hourly rate of water yield is not a suitable parameter to compare the performance of the system. Because there is a delay effect of solar radiation on water production rate due to initial startup thermal inertial. In addition, the recorded amount of water in a specific hour is not necessarily generated under the solar radiation flux during the same hour. Therefore, the daily total water yield and daily distillation

efficiency would present more reliable estimates about the system performance. The daily distillation efficiency of the FHSS was approximately 36 %, somewhat greater than the that of RPSS (18%). This is about 100% improvement in the distillation efficiency compared to the RPSS system.

4.2. Indoor salt diffusion experiment

Fig. 8 depicts the experiment for investigating the potential of the basin in the diffusion of salt dispersed on top of the basin into the bulk water. In conventional solar stills, salt residuals are accumulated on the

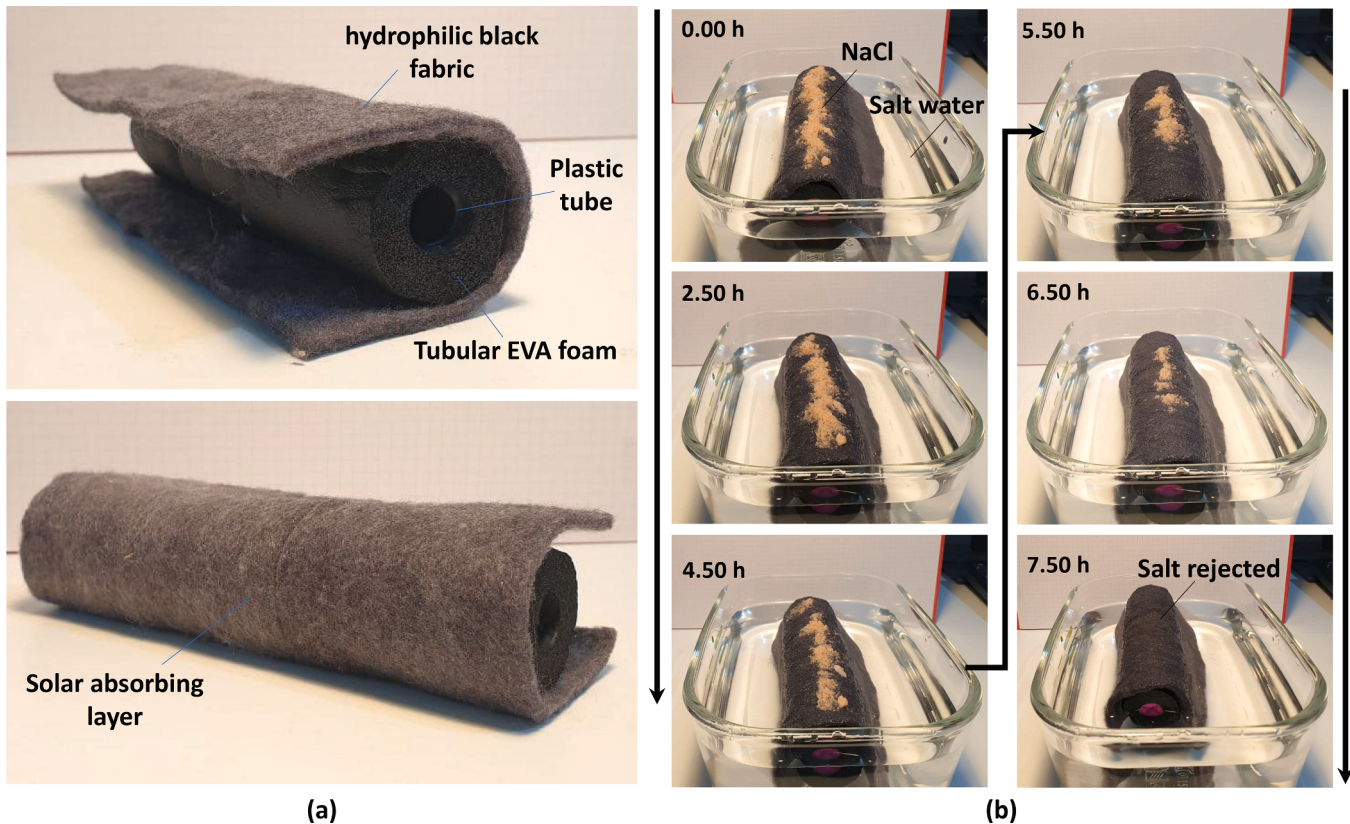


Fig. 8. Indoor salt-diffusion experiment. (a) the multi-layer structure of the basin. (b) the rejection progression of the salt dispersed on top of the basin into a tray containing water with 4.0 wt% salt concentration.

surface of the basin as a consequence of water evaporation which requires to manually remove from time to time. In this indoor experiment, 11 gm of salt was placed on a small piece of the basin structure with an area of 55 cm² floating in a tray that contains water with 4.0 wt% salt. It took around 7.5 h for the salt to dissolve into the water and disappear from the surface. The salt dissolving potential of the current basin structure is well and enough to completely remove the residual salt during the night while the system is floating and to make the basin clean and ready for operation on the next day.

4.3. Cost analysis

The cost of materials of the FHSS system is reported in Table 4. The total cost of the FHSS system was calculated to be \$213. The cost of the acrylic dome itself is the most considerable cost for the solar still as it was a custom-made order. This cost is expected to reduce (potentially to around \$10) if mass-produced. The unit water cost analysis considering 8 years of system operation life is provided in Table 5. The Capital

Table 4

List of the raw materials cost and labour cost (in USD) for the FHSS system.

Components	Specifications	Cost (USD)
Hemispherical Cover	Clear Acrylic (700 mm Dia.)	68.00
Hydrophilic fabric wick	Cellulose, Zorb	11.00
Expanded porous foam	Tubular EVA (28 mm Dia.)	6.00
Condensing coils	Annealed Copper (3/8"(9.5 mm) Dia.)	32.00
Air vacuum pump	15 W, 40 L min ⁻¹	15.00
Connector and clamps	Stainless Steel	3.50
Pipeline	Polyvinyl	5.00
Framework	Polyethylene tubes	12.00
Labour	15 hrs (rate of \$4 per hour)	60.00
Total costs		212.50

Table 5

The unit water cost analysis breakdowns (in USD) for Floating Hemispherical Solar Still (FHSS) and RPSS.

Parameter	RPSS	FHSS
Operation life, a	10	8
Interest rate, %	4.0	4.0
Capital cost, \$	249	213
Net Aperture area for solar, m ²	0.48	0.35
Salvage value, \$	27	64
Capital recovery factor	0.12	0.15
Sinking-fund factor	0.08	0.11
Annual Salvage Value, \$	2.25	6.95
First annual cost, \$	30.70	31.64
Annual maintenance cost, \$	4.60	1.58
Annual cost, \$	33.1	26.3
Average daily water yield, L	1.03	1.52
Annual yield (Ave. daily yield × 365), L	375.9	554.8
Unit water cost, ¢ L ⁻¹	8.8	4.7

Recovery Factor (CRF), Sinking-Fund Factor (SFF), First Annual Cost (FAC), Annual cost (AC), Salvage Value (SV), Annual Salvage Value (ASV), and the unit water cost (UWC) were calculated by using Eqs. (2)–(7) [46].

$$CRF = i (1 + i)^n / [(1 + i)^n - 1] \quad (2)$$

$$FAC = P \cdot CRF \quad (3)$$

$$SV = 0.5 CRM \quad (4)$$

$$SFF = i / [(1 + i)^n - 1] \quad (5)$$

$$ASV = SV \cdot SFF \quad (6)$$

Table 6

The uncertainty values of the performance parameters for FHSS and RPSS.

System	RPSS			FHSS		
Variable	m_d (L d^{-1})	I_d (MJ m^{-2})	η (%)	m_d (L d^{-1})	I_d (MJ m^{-2})	η (%)
Value	1.025	8.483	17.8	1.520	8.483	35.6
Uncertainty	± 0.010	± 0.424	± 0.57	± 0.015	± 0.424	± 1.15

$$AC = FAC + AMC + AEC - ASV \quad (7)$$

where, i is the interest rate, P the capital cost, and n system operation life. The annual maintenance cost (AMC) of the FHSS system is predicted at 5% FAC. The AMC and operation life for the RPSS are taken as 15% of FAC and 10 years as suggested in ref. [46], respectively. The salvage value (SV) is assumed to be at 50% of the cost of reusable materials (CRM). The annual electricity cost (AEC) for the operation of the low power air pump is assumed to be neglected, and it is proposed to be supplied by a small size PV solar panel.

According to the cost analysis, the life cycle cost of one litre of water generated by the FHSS is estimated to be 4.7 ¢ L^{-1} . The estimated unit water cost for RPSS built with the total cost of \$249 for the experiments is 8.8 ¢ L^{-1} . The unit water cost of FHSS shows 46 % reduction compared to the RPSS. The comparison of the unit water cost of the current system among previous studies on similar solar stills is elaborated in Section 4.5.

4.4. Uncertainty analysis

The reliability of the estimated performance parameters was examined by an uncertainty analysis. The Kline and McClintock method was used to determine the uncertainty of the performance parameters calculated from the measured quantities as [47]:

$$u_c(y) = \sqrt{\sum_{i=1}^n \left(\frac{\partial y}{\partial x_i} \right)^2 u^2(x_i)} \quad (8)$$

where, $u_c(y)$ is the uncertainty value of the performance parameter y , y is a function of quantities measured directly in the experiment given by $y=f(x_1, x_2, \dots, x_n)$, and $u(x_i)$ is the measurement uncertainty of quantity x_i .

According to the outdoor measurement results in Section 4.1 and the instruments uncertainties in Table 2, the uncertainties of performance parameters are provided in Table 6. According to the calculations, the total uncertainty of the distilled water generation efficiency of FHSS system is $\pm 1.15\%$.

4.5. Comparison of the current research with existing floating solar stills

Table 7 compares the water yield, distillation efficiency, capital cost, and unit water cost of the current work with similar experimental studies on floating solar stills, natural vacuum desalination (NVD)

systems, and hemispherical solar stills. The current study shows significantly higher distillation efficiency and water yield of 36 % and 1.52 L d^{-1} among existing floating solar stills; however, the natural vacuum desalination system in ref [41] which works under the high vacuum pressure of 23.4 kPa and with the solar heat supplied by evacuated tube collectors (ETC) has reached 47.6%. The tubular platform of the basin at the system proposed in this article creates a rounded texture on the basin surface making an extra interface area for the evaporation compared to the floating solar stills listed in Table 7. This enables a higher water yield for the same dimensions of the basin. In many of the systems provided in the table, the residual salt remaining on the basin requires periodic cleaning. This increases the maintenance cost of these systems significantly; however, some studies excluded it from their UWC estimations. The cost of double-slope floating PSS studied in Ref. [11] was reported to be only \$3 which means a UWC of 0.4 ¢ L^{-1} ; however, the lifetime for this system was about two years which is considerably lower than the estimated lifetime of the FHSS presented in this article.

4.6. Existing shortcomings and future considerations

Aside from the advantages of the developed system, the new design has some shortcomings which should be addressed in future studies. The creation of water droplets on the cover of a solar still, due to vapour condensation, partially obstructs the incident solar radiation from reaching the basin surface. Therefore, one of the challenges in this work was to reduce the condensation of the vapour on the hemispherical cover as much as possible by directing it to the condensing coils where approximately 77% of the condensate was collected. Additionally, attempts were made to improve the effectiveness of the hemispherical cover in collecting water droplets from the cover surface at a faster rate to allow more solar radiation to reach the basin interface. In this regard, different types of commercially available antifog and water repellent coating products were applied on the inner surface of the hemispherical cover. The outcome was marginally effective with the water repellent coating; however, the effect of the coating was temporary and lasted no longer than four to five hours. It is anticipated that a longer life anti-fog coating would further improve the production of the FHSS and is a subject for future investigation and development.

Furthermore, the relatively high temperature of up to 45°C around the condensing coils in FHSS system is of concern due to the induced heat loss via the wick fabric into the bulk water. This concern needs to be considered in future studies via an efficient design of the basin structure.

Table 7

Performance parameters of various solar stills.

System description	Water yield (L d^{-1})	Area (m^2)	η (%)	Capital cost (USD)	Lifetime(a)	UWC(¢ L^{-1})
Hemispherical Floating Solar Still (present)	1.52	0.35	35.7	213	8	4.7
Commercial portable PSS (Watercone) [48]	0.5–1.0	0.38	19.3	24	3–5	–
Commercial floating PSS (Aquamate) [49]	0.34	0.34	–	239	2	106.6
Double-slope floating PSS [11]	0.75	0.30	22.0	3	2	0.4
Single-slope floating PSS [12]	0.83	0.34	–	76.5	5	6.6
Double-slope floating PSS [14]	1.50	1.00	15.7	43.5	5	2.1
Hemispherical CPSS [50]	3.65	1.00	34.0	210	10	1.8
NVD with solar ETC [41]	1.36	0.17	47.6	243	10	9.4

5. Conclusions

The multi-layer basin made of low-cost hydrophilic cellulose wick fabric and tubular EVA insulation foam created a suitable localized solar heating at the interface and obtained a maximum temperature of 84°C. The rounded geometry of the basin surface created by the tubular platform provided a larger interface area for water evaporation compared to existing floating solar stills designs (e.g. Ref [11,12]). The structure showed a sufficient salt rejecting rate through the capillary water circulation to continuously clean the system from residual salt accumulation. The hemispherical cover on top of the basin provided a considerable surface for water vapour condensation which was found to collect 23 % of the total distilled water; however, the majority of the vapour was condensed in the submerged copper coils coupled with the basin structure. The system was found to be capable of generating distilled water at a daily rate of 4.3 L m⁻² d⁻¹ with the distillation efficiency of 36 % during summer in Melbourne. This was 64% higher than the water yield of the reference passive solar still tested alongside the floating solar still.

This system is expected to have a lower maintenance cost compared to conventional passive solar stills because it does not require a water pump to supply the water into the basin and does not warrant as much periodic cleaning. The life cycle cost per litre of potable water generated by this system is estimated to be 4.7 ¢ L⁻¹ which showed a substantial reduction of 46% when compared to the tested reference passive solar still and less cost than that of similar solar stills reported in the literature. With the ease of fabrication, low-cost, and ease of use, the proposed FPSS is therefore a feasible option to address the water security challenge in water-stressed communities in remote or disaster-stricken areas with no access to an energy infrastructure.

CRediT authorship contribution statement

Milad Mohsenzadeh: Conceptualization, Data curation, Formal analysis, Investigation, Methodology, Software, Visualization, Writing – original draft. **Lu Aye:** Funding acquisition, Project administration, Resources, Supervision, Writing – review & editing. **Philip Christopher:** Supervision, Validation, Writing – review & editing.

Declaration of Competing Interest

The authors declare the following financial interests which may be considered as potential competing interests: A patent application with the Intellectual Property right number 2021903521 has been filed covering the work in this article including the specifications of the developed innovative system and the relevant datasets.

Acknowledgements

Milad Mohsenzadeh would like to gratefully acknowledge the financial support for this research provided by The University of Melbourne through the Melbourne Research Scholarship award. We also would like to acknowledge the Facilities and OH&S team at the Faculty of Engineering and Information Technology for their arrangements to access the facilities and the test site under COVID-19 restrictions.

References

- [1] Shiklomanov IA, Rodda JC, editors. *World water resources at the beginning of the twenty-first century*. Cambridge University Press; 2004.
- [2] Gude VG. Desalination and water reuse to address global water scarcity. *Rev Environ Sci Bio/Technol* 2017;16(4):591–609. <https://doi.org/10.1007/s11157-017-9449-7>.
- [3] Hasan E, Tarhule A, Hong Y, Moore B. Assessment of physical water scarcity in Africa using GRACE and TRMM satellite data. *Remote Sens* 2019;11(8):904. <https://doi.org/10.3390/rs11080904>.
- [4] Kim J, Park K, Yang DR, Hong S. A comprehensive review of energy consumption of seawater reverse osmosis desalination plants. *Appl Energy* 2019;254:113652. <https://doi.org/10.1016/j.apenergy.2019.113652>.
- [5] Dsilva Winfred Rufuss D, Iniyani S, Suganthi L, Davies PA. Solar stills: A comprehensive review of designs, performance and material advances. *Renew Sustain Energy Rev* 2016;63:464–96. <https://doi.org/10.1016/j.rser.2016.05.068>.
- [6] Zhang L, Xu Z, Bhatia B, Li B, Zhao L, Wang EN. Modeling and performance analysis of high-efficiency thermally-localized multistage solar stills. *Appl Energy* 2020;266:114864. <https://doi.org/10.1016/j.apenergy.2020.114864>.
- [7] Xu J, Wang Z, Chang C, Fu B, Tao P, Song C, et al. Solar-driven interfacial desalination for simultaneous freshwater and salt generation. *Desalination* 2020; 484:114423. <https://doi.org/10.1016/j.desal.2020.114423>.
- [8] Tao P, Ni G, Song C, Shang W, Wu J, Zhu J, et al. Solar-driven interfacial evaporation. *Nat Energy* 2018;3(12):1031–41. <https://doi.org/10.1038/s41560-018-0260-7>.
- [9] Xu J, Wang Z, Chang C, Fu B, Tao P, Song C, et al. Solar-driven interfacial desalination for simultaneous freshwater and salt generation. *Desalination* 2020; 484:114423. <https://doi.org/10.1016/j.desal.2020.114423>.
- [10] Nafei AS, Abdelkader M, Abdelfataip A, Mabrouk AA. Enhancement of solar still productivity using floating perforated black plate. *Energy Convers Manage* 2002; 43(7):937–46. [https://doi.org/10.1016/S0196-8904\(01\)00079-6](https://doi.org/10.1016/S0196-8904(01)00079-6).
- [11] Ni G, Zandavi SH, Javid SM, Boriskina SV, Cooper TA, Chen G. A salt-rejecting floating solar still for low-cost desalination. *Energy Environ. Sci.* 2018;11(6): 1510–9. <https://doi.org/10.1039/C8EE00220G>.
- [12] Liu Z, Song H, Ji D, Li C, Cheney A, Liu Y, et al. Extremely cost-effective and efficient solar vapor generation under nonconcentrated illumination using thermally isolated black paper. *Global Challenges* 2017;1(2):1600003. <https://doi.org/10.1002/gch2.201600003>.
- [13] Wang Q, Zhu Z, Wu G, Zhang X, Zheng H. Energy analysis and experimental verification of a solar freshwater self-produced ecological film floating on the sea. *Appl Energy* 2018;224:510–26. <https://doi.org/10.1016/j.apenergy.2018.05.010>.
- [14] Chen S, Zhao P, Xie G, Wei Y, Lyu Y, Zhang Y, et al. A floating solar still inspired by continuous root water intake. *Desalination* 2021;512:115–33. <https://doi.org/10.1016/j.desal.2021.115133>.
- [15] Sharshir SW, Algazzar AM, Elmaadawy KA, Kandeel AW, Elkadeem MR, Arunkumar T, et al. New hydrogel materials for improving solar water evaporation, desalination and wastewater treatment: A review. *Desalination* 2020;491:114564. <https://doi.org/10.1016/j.desal.2020.114564>.
- [16] Li Z, Wang C, Lei T, Ma H, Su J, Ling S, et al. Arched bamboo charcoal as interfacial solar steam generation integrative device with enhanced water purification capacity. *Adv Sustain Syst* 2019;3(4):1800144. <https://doi.org/10.1002/adsu.201800144>.
- [17] Janarthanan B, Chandrasekaran J, Kumar S. Performance of floating cum tilted-wick type solar still with the effect of water flowing over the glass cover. *Desalination* 2006;190(1–3):51–62. <https://doi.org/10.1016/j.desal.2005.08.005>.
- [18] El-Agouz SA. Experimental investigation of stepped solar still with continuous water circulation. *Energy Convers Manage* 2014;86:186–93. <https://doi.org/10.1016/j.enconman.2014.05.021>.
- [19] Singh DB, Yadav JK, Dwivedi VK, Kumar S, Tiwari GN, Al-Helal IM. Experimental studies of active solar still integrated with two hybrid PVT collectors. *Sol Energy* 2016;130:207–23. <https://doi.org/10.1016/j.solener.2016.02.024>.
- [20] Jamil B, Akhtar N. Effect of specific height on the performance of a single slope solar still: an experimental study. *Desalination* 2017;414:73–88. <https://doi.org/10.1016/j.desal.2017.03.036>.
- [21] Agrawal A, Rana RS, Srivastava PK. Heat transfer coefficients and productivity of a single slope single basin solar still in Indian climatic condition: experimental and theoretical comparison. *Resour-Effic Technol* 2017;3(4):466–82. <https://doi.org/10.1016/j.refit.2017.05.003>.
- [22] Elango T, Kalidas Murugavel K. The effect of the water depth on the productivity for single and double basin double slope glass solar stills. *Desalination* 2015;359: 82–91. <https://doi.org/10.1016/j.desal.2014.12.036>.
- [23] Kim K, Yu S, Kang S-Y, Ryu S-T, Jang J-H. Three-dimensional solar steam generation device with additional non-photothermal evaporation. *Desalination* 2019;469:114091. <https://doi.org/10.1016/j.desal.2019.114091>.
- [24] Ghasemi H, Ni G, Marconnet AM, Loomis J, Yerci S, Miljkovic N, et al. Solar steam generation by heat localization. *Nat Commun* 2014;5(1):1–7. <https://doi.org/10.1038/ncomms4449>.
- [25] Liu G, Chen T, Xu J, Yao G, Xie J, Chen Y, et al. Salt-rejecting solar interfacial evaporation. *Cell Rep Phys Sci* 2021;2(1):100310. <https://doi.org/10.1016/j.xcrp.2020.100310>.
- [26] Ma Q, Yin P, Zhao M, Luo Z, Huang Y, He Q, et al. MOF-based hierarchical structures for solar-thermal clean water production. *Adv Mater* 2019;31(17): 1808249. <https://doi.org/10.1002/adma.201808249>.
- [27] Wu L, Dong Z, Cai Z, Ganapathy T, Fang NX, Li C, et al. Highly efficient three-dimensional solar evaporator for high salinity desalination by localized crystallization. *Nat Commun* 2020;11(1):1–12. <https://doi.org/10.1038/s41467-020-14366-1>.
- [28] Huang J, Hu Y, Bai Y, He Y, Zhu J. Novel solar membrane distillation enabled by a PDMS/CNT/PVDF membrane with localized heating. *Desalination* 2020;489: 114529. <https://doi.org/10.1016/j.desal.2020.114529>.
- [29] Wilson HM, Rahman S, Parab AE, Jha N. Ultra-low cost cotton based solar evaporation device for seawater desalination and waste water purification to produce drinkable water. *Desalination* 2019;456:85–96. <https://doi.org/10.1016/j.desal.2019.01.017>.

- [30] Zhou X, Zhao F, Guo Y, Zhang Y, Yu G. A hydrogel-based antifouling solar evaporator for highly efficient water desalination. *Energy Environ Sci* 2018;11(8):1985–92. <https://doi.org/10.1039/C8EE00567B>.
- [31] Lv B, Gao C, Xu Y, Fan X, Xiao J, Liu Y. A self-floating, salt-resistant 3D Janus radish-based evaporator for highly efficient solar desalination. *Desalination* 2021;510:115093. <https://doi.org/10.1016/j.desal.2021.115093>.
- [32] Ni G, Li G, Boriskina SV, Li H, Yang W, Zhang T, et al. Steam generation under one sun enabled by a floating structure with thermal concentration. *Nat Energy* 2016;1(9):1–7. <https://doi.org/10.1038/nenergy.2016.126>.
- [33] Li Y, Hong W, Li H, Yan Z, Wang S, Liu X, et al. Solar absorber with tunable porosity to control the water supply velocity to accelerate water evaporation. *Desalination* 2021;511:115113. <https://doi.org/10.1016/j.desal.2021.115113>.
- [34] Liu H, Chen C, Chen G, Kuang Y, Zhao X, Song J, et al. High-performance solar steam device with layered channels: artificial tree with a reversed design. *Adv Energy Mater* 2018;8(8):1701616. <https://doi.org/10.1002/aenm.201701616>.
- [35] He S, Chen C, Kuang Y, Mi R, Liu Y, Pei Y, et al. Nature-inspired salt resistant bimodal porous solar evaporator for efficient and stable water desalination. *Energy Environ Sci* 2019;12:1558–67. <https://doi.org/10.1039/C9EE00945K>.
- [36] Zhao L, Wang P, Tian J, Wang J, Li L, Xu L, et al. A novel composite hydrogel for solar evaporation enhancement at air-water interface. *Sci Total Environ* 2019;668:153–60. <https://doi.org/10.1016/j.scitotenv.2019.02.407>.
- [37] Gao M, Zhu L, Peh CK, Ho GW. Solar absorber material and system designs for photothermal water vaporization towards clean water and energy production. *Energy Environ Sci* 2019;12(3):841–64. <https://doi.org/10.1039/C8EE01146J>.
- [38] Li R, Shi Y, Alsaedi M, Wu M, Shi L, Wang P. Hybrid hydrogel with high water vapor harvesting capacity for deployable solar-driven atmospheric water generator. *Environ Sci Technol* 2018;52(19):11367–77. <https://doi.org/10.1021/acs.est.8b02852>.
- [39] Li X, Xu G, Peng G, Yang N, Yu W, Deng C. Efficiency enhancement on the solar steam generation by wick materials with wrapped graphene nanoparticles. *Appl Therm Eng* 2019;161:114195. <https://doi.org/10.1016/j.applthermaleng.2019.114195>.
- [40] Al-Kharabsheh S, Goswami DY. Experimental study of an innovative solar water desalination system utilizing a passive vacuum technique. *Sol Energy* 2003;75(5):395–401. <https://doi.org/10.1016/j.solener.2003.08.031>.
- [41] Abbaspour MJ, Feagh M, Shafii MB. Experimental examination of a natural vacuum desalination system integrated with evacuated tube collectors. *Desalination* 2019;467:79–85. <https://doi.org/10.1016/j.desal.2019.06.004>.
- [42] Xie G, Chen W, Yan T, Tang J, Liu H, Cao S. Three-effect tubular solar desalination system with vacuum operation under actual weather conditions. *Energy Convers Manage* 2020;205:112371. <https://doi.org/10.1016/j.enconman.2019.112371>.
- [43] Rashid A, Ayhan T, Abbas A. Natural vacuum distillation for seawater desalination—A review. *Desalin Water Treat* 2016;57(56):26943–53. <https://doi.org/10.1080/19443994.2016.1172264>.
- [44] Cengel YA, Boles MA. *Thermodynamics: An Engineering Approach Sixth Edition (SI Units)*. New York: McGraw-Hill; 2007.
- [45] Mohsenzadeh M, Aya L, Christopher P. A review on various designs for performance improvement of passive solar stills for remote areas. *Sol Energy* 2021;594–611. <https://doi.org/10.1016/j.solener.2021.09.086>.
- [46] Fath HES, El-Samanoudy M, Fahmy K, Hassabou A. Thermal-economic analysis and comparison between pyramid-shaped and single-slope solar still configurations. *Desalination* 2003;159(1):69–79. [https://doi.org/10.1016/S0011-9164\(03\)90046-4](https://doi.org/10.1016/S0011-9164(03)90046-4).
- [47] Kline SJ, McClintock FA. Describing uncertainties in single-sample experiments. *Mech Eng* 1953;75:3–8.
- [48] Watercone® Inc., n.d. <http://www.watercone.com/> (accessed June 10, 2020).
- [49] Aquamate®. <https://www.landfallnavigation.com/aquamate-solar-still.html> (accessed May 10, 2021).
- [50] Arunkumar T, Jayaprakash R, Denkenberger D, Ahsan A, Okundamiya MS, Kumar S, et al. An experimental study on a hemispherical solar still. *Desalination* 2012;8:286–342. <https://doi.org/10.1016/j.desal.2011.11.047>.